

Overbounding I-free errors based on Bayesian Gaussian mixture model for ground-based augmentation system

Sheher Banu, Hameem Shanavas

Department of Electronics and Communication Engineering, MVJ College of Engineering, Bangalore, affiliated to Visvesvaraya Technological University, Belagavi, India

Article Info

Article history:

Received Oct 4, 2023

Revised Jan 20, 2024

Accepted Jan 23, 2024

Keywords:

Dual-frequency

Gaussian mixture model

Ground-based augmentation system

I-free-based filtering algorithm

Single-frequency

ABSTRACT

A dual-frequency measurement is employed in conjunction with an innovative I-free filtering technique for mitigating the primary sources of I-free influence on ground-based augmentation systems (GBAS) to safeguard the reliability of GBAS. The protective level achieved through the conventional Gaussian overbounding approach that are considered as much conventional technique. This adherence to tradition results in decreased reliability and a higher likelihood of false alarms. In contrast, the utilization of the I-free algorithm contributes to reducing errors associated with dual-frequency measurements. This paper proposes the overbounding process according to Bayesian Gaussian mixture model (GMM) for maintaining I-free-based GBAS range error. The Bayesian GMM is utilized for single-frequency model errors to examine the ambiguity estimations. The Monte Carlo (MC) simulation is established for defining estimated GMM assurance level accuracy which is attained through the general estimation method. Then, the last Bayesian GMM which is utilized for overbounding I-free error distribution is investigated. According to the property of convolution invariance, the vertical protection in position field is determined without presenting difficult numerical calculations.

This is an open access article under the [CC BY-SA](https://creativecommons.org/licenses/by-sa/4.0/) license.



Corresponding Author:

Sheher Banu

Department of Electronics and Communication Engineering, MVJ College of Engineering, affiliated to Visvesvaraya Technological University

Bangalore-560067, India

Email: sheherbanu@mvjce.edu.in

1. INTRODUCTION

The ground-based augmentation system (GBAS) is a technology designed to enhance the accuracy and consistency of air navigation during landing. This technique delivers innovative civil aviation facilities to improve accuracy, availability, integrity, and endurance [1]. Truthfulness is the main aspect of indicating the security of precision methods at airports. It refers to its ability to alert when the output is not reliable. The reference station of GBAS broadcasts disparity correlation with truthfulness parameters [2], [3]. The GBAS verifies the integrity in three ways: delivering disparity correlations of local-area and elimination of general-mode errors; delivering the authorized user through a personalized monitor for system faults; and enabling the user to create a residual error bound to make navigation actions [4]. Due to free electrons, the ionospheric delay along the path of the Global Navigation Satellite System (GNSS) signal is circulated consistently under normal conditions [5]. Whenever GNSS signals travel with the circulated ionosphere, a severe error that potentially compromises the truthfulness of GBAS is observed [6]. The ionospheric threat anomaly is displayed as a wavefront wedge and spatial linear semi-infinite at a fixed speed in mid-latitude areas [7]. The space-based augmentation system (SBAS) communicates real-time error correlations through geostationary

satellites. This SBAS utilizes a global positioning system (GPS) signal which provides an easy way for SBAS signal to GPS receiver without the substantial modifications [8], [9]. Additionally, SBAS generates truthfulness in data correlation for error bound positions. This truthfulness data contains covariance errors of each correlation, clock, orbit and ionosphere [10]. These covariances are utilized to define weight measurements during the position method and are employed to distinguish the error bound calculations [11]. By utilizing this error bound, the SBAS-based GNSS establishes whether or not to employ GNSS [12]. Further, for developing a scientific algorithm, a weighed mean model is employed to define output scores for positioning the SBAS. Then, ionospheric correction is attained from the local estimated ionospheric delay [13]. During the ionospheric delay, the spatial correlation is high, where a regional map containing SBAS map exposure which is enlarged through spatial prediction technique [14]. There are two analyses on this map, temporal and prediction, which consume the past and interior observations [15]. In the recent years, it is seen that over-bounding relies on localization for defining its location and pose which subsequently aids the path planning and navigation processes [16]. The localization techniques such as cooperative positioning, field measure from sensors and range-based techniques are developed to attain high-level positioning accuracy [17]. However, the sensors deployed in this localization system generate measurement errors like single-point solution in GPS and offset drifts in the inertia sensors [18].

Gao *et al.* [19] implemented a Gaussian mixture model (GMM) for handling samples from ionosphere-free based GBAS errors. The GMM was applied to individual-frequency errors which examined the vagueness. In addition, Monte Carlo was executed to determine the evaluated GMM assurance level accuracy attained by the common estimation method. A road test displayed that the GMM overbound secured vertical protection levels (VPLs), with better computational rate compared to various non-Gaussian overbounds. However, the developed method had multiway errors which required an innovative degree of arithmetical correlation among frequencies. Lee *et al.* [20] developed an optimum parameter rise to improve the accessibility of individual-frequency GBAS for smart air transportation. The performance of three geometry-screening algorithms was related to four airports with low and mid-latitude areas. The target and optimum parameter performance were parallel in terms of availability. The optimal parameter minimized computational rate through the target parameter. Hence, the developed method needed to enhance the GBAS availability for designing a much more accurate and lower conventional ionospheric model which considers the features of equatorial plasma bubbles (EPBs). Maurer *et al.* [21] introduced the flight trial demonstration of secure GBAS through L-band digital aeronautical communications system (LDACS). The GBAS information was genuine with TESLA protocol secure GBAS, and the secured message was communicated to the aircraft by LDACS. The LDACS was applied to very high frequency (VHF) data broadcast (VDB) which offered a minimum of ten times in data-rate ability. It provided a sufficient data rate for broadcasting secured GBAS data while providing spare ability for various services on similar channels. This method enhanced the data rate and improved the range and cyber security. Lee *et al.* [22] suggested a viability of GPS L2C Signals for space service volume (SSV) receivers on SBAS-Geostationary Orbit (GEO) satellites. The satellite perceptibility, precision dilution, and navigation error are enhanced when the GPS L2C signal was deployed in GEO satellites over arithmetical simulation. The evaluation assumed that the Ifree correction was accomplished with exterior information, and the signal transmitted over Ifree was omitted. Nonetheless, decrease in geometric dilution of precision (GDOP) was higher, while navigation errors inclined to reduce through the threshold.

Bang and Lee [23] presented the under-sampled ionospheric irregularity threat parameterization by 3D model for SBAS. This methodology was presented for under-sampled ionospheric threats to reduce the magnitude of grid ionospheric vertical errors (GIVE). An under-sampled threat model was created with a developed 3D metric set and historical ionospheric storm data from GNSS stations in South Korea. Nonetheless, the introduced method was required to be comprised of a performance investigation behavior of enhancement by applying a new threat model for high-range station establishments. Wang *et al.* [24] recommended the methodology of signal quality monitor (SQM) for BeiDou navigation satellite System (BDS) B1C/B2a signals, which simply extended to dual-frequency integrations of various GNSS core patterns. The comparison of the SQM algorithm's performance was performed based on convolutional multi-correlator and emerging Chip Domain Observables. Its exhaustive iteration design was analyzed by including the algorithm's practices through enhancing code-phase length and sample frequency. Additionally, the metric interpretation was performed for promoting total performance by conserving the low execution difficulty. Jardak and Jault [25] implemented a probable Low Earth Orbit (LEO) satellite-based opportunistic navigation for high-dynamic applications. The less-duration mission was expected to overcome the performance of optimum navigation which was used to estimate probable LEO space vehicle (SV) signals of opportunity (SOP) for large-dynamic vehicles. This Doppler shift information was more illustrative than the attained error distribution among the satellite and user terminals. These results illustrate the possibility of LEO SV signals for navigation of high-dynamic vehicles in the GNSS environment. But the huge satellite orbit errors and clock drifts were the limiting factors of Doppler shift-based positioning performance. From

the overall analysis, the existing methods have limitations such as that the multiway errors required an innovative degree of arithmetical correlation among frequencies. They need to enhance the GBAS availability for designing a much more accurate and lower conventional ionospheric model. They need to enhance the error rate, range and cyber security, along with the navigation errors inclined to reduce with the threshold. They require to comprise a performance investigation behavior of enhancement, through applying a new threat model for high-range station establishments. The major contributions of this research are as follows: i) This paper proposes the overbounding process based on the Bayesian Gaussian mixture model to maintain I_{free}-based GBAS range error; ii) I_{free}-based protection with Bayesian GMM overbounding is utilized to estimate the protection levels that enhance the accuracy without enhancing the computational complexity; and iii) The influence of errors mainly contains satellite position errors, velocity errors, and clock drift.

The rest of the manuscript is organized as follows: section 2 illustrates the proposed method. The overbounding I_{free}-errors based on Bayesian GMM are presented in section 3. The results and discussion are illustrated in section 4. Section 5 describes the conclusion of this paper.

2. PROPOSED METHOD

The process of overbounding I_{free}-based GBAS based on GMM is described in this section. The suggested method has a possibility of overbounding I_{free}-based errors securely. Initially, a block diagram of the methodology is presented, then the details required to achieve a redesigned closed-form GMM overbounding to minimize the progressiveness are studied. The process of I_{free} filter is presented in Figure 1.

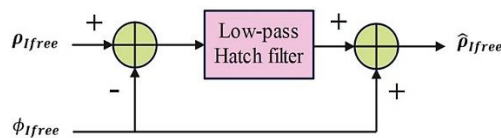


Figure 1. I_{free} filtering process

3. OVERBOUNDING I_{FREE}-ERRORS BASED ON GAUSSIAN MIXTURE MODEL

3.1. Process of overbounding I_{free}-based error

The I_{free} filtering isolates ionospheric first-order effects with the I_{free} integrations of global navigation satellite system (GNSS) calculations from dual-frequencies. The I_{free} filtering algorithm's input is shown in (1) and (2),

$$\rho_{I_{free}} = \rho_{f1} - \frac{1}{\zeta}(\rho_{f1} - \rho_{f2}) \quad (1)$$

$$\phi_{I_{free}} = \phi_{f1} - \frac{1}{\zeta}(\phi_{f1} - \phi_{f2}) \quad (2)$$

where, ρ and ϕ are the range and carrier-phase measurements, respectively. ζ is estimated as $\zeta = 1 - f_1^2/f_2^2$. The low-pass filter is utilized for reducing higher-frequency noise in input calculations. The filtering output is shown in (3),

$$\hat{\rho}_{I_{free}} = R + \left(\varepsilon_1 - \frac{1}{\zeta}(\varepsilon_1 - \varepsilon_2) \right) + \frac{1}{\zeta}IFB \quad (3)$$

where, R is the carrier-phase and code measurements of all common terms which contain true distance among the user and satellites, satellite and recipient clock biased, and tropospheric interruption. ε are the errors in filtering which include thermal noise and multipath errors. IFB represents the inter frequency bias. The I_{free}-based errors are designed through the integration of dual frequencies that produce higher individual-frequency errors. Among them, one can evaluate overbounding directly according to I_{free}-based filtering quantities. A corresponding illustration of I_{free} filtering and overbounding is presented in Figure 2.

Here, Figure 1 is transformed into Figure 2(a) because I_{free} filtering is a linear system. With the help of additivity and homogeneousness properties, I_{free}-based GBAS is degraded in dual components. Furthermore, the dimensions are integrated when transmitting with a similar low-pass Hatch filter. The

overall process of overbounding is presented in Figure 2(b) according to the equal I_{free} filtering algorithm. The range error overbounding model (REOM) and range error distribution model (REDM) are recognized by utilizing every frequency error. Next, I_{free} -based GBAS of REOM is attained by folding dual individual-frequency REOM linearly. The I_{free} -based overbounding depends on an error of independent derivative from dual-frequency measurements. The overbounding is not derivative from the last I_{free} -based error estimation directly. If one frequency measurement is inhibited with another frequency it is viable to be modeled and received during sample collection.

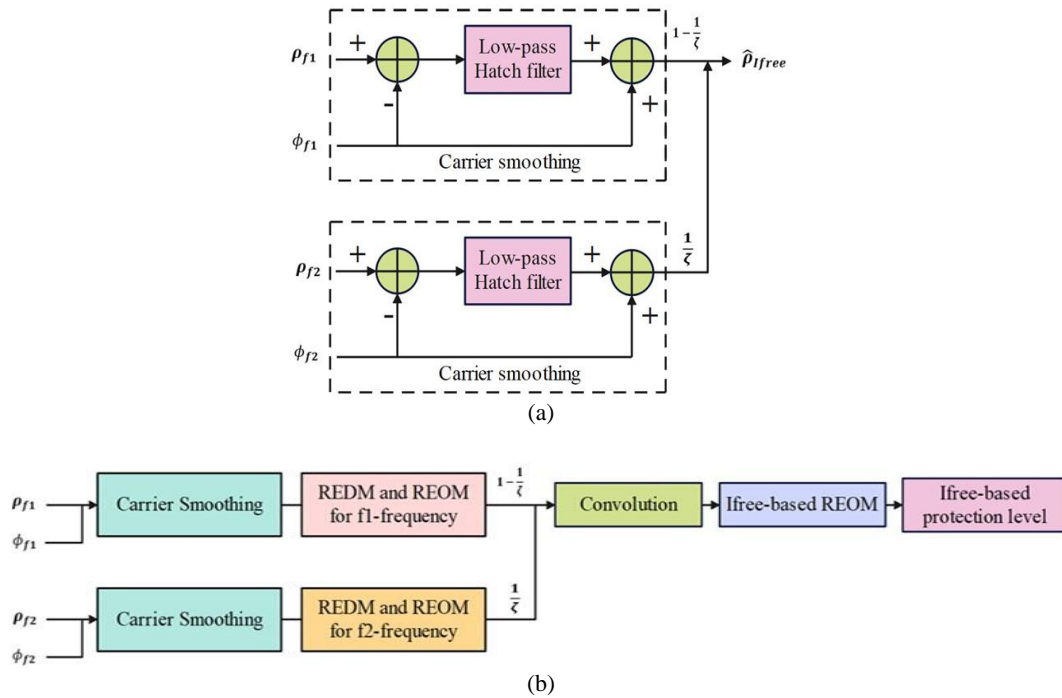


Figure 2. Corresponding figure of I_{free} filtering process (a) A corresponding illustration of I_{free} filtering process. (b) The I_{free} -based overbounding in GBAS

3.2. Single-frequency REDM formation

It describes the errors associated with measuring a quantity within a specified frequency range of band. The error displays a large tail when the elevation is minor. Due to the overbounding cumulative distribution function (CDF) [26] necessitating the location parameter μ is zero while the dual-component GMM REDM is recognized and specified in (4).

$$p(y) = \omega_1 \varphi(y; 0, \sigma_1) + \omega_2 \varphi(y; 0, \sigma_2) \tag{4}$$

where $\omega_1 + \omega_2 = 1$. The three reasons for selecting dual-component GMM:

- a. This model reduces the number of components by distributing adequate flexibility. In this, one component defines the core while the other defines tails.
- b. Overbounding a multi-component model with dual-component model.
- c. This model avoids nonconvergence and overfitting problems. The suggested model is utilized to evaluate the parameters, where the heavy tail is inattentive for higher upgradation, and the distributed error is attended for Gaussian distribution. At this moment, the expectation-maximization (EM) crashes for convergence, thus the understandable Gaussian overbounding is selected.

3.3. Single-frequency REOM formation

The REOM construction is essential to substitute present parameters in REDM through bounds. This model provides an upper bound or an approximation of the maximum error that occurs within the defined frequency band. In order to enhance and reduce the parameter scores, the REDM parameter calculated through the EM algorithm is overbounding. The σ_1 is greater than σ_2 , then the overbounding model structure is shown in (5),

$$p_{OB}(y) = (\omega_1 + \Delta\omega)\varphi(y; 0, \sigma_1 + \Delta\sigma_1) + (\omega_2 + \Delta\omega)\varphi(y; 0, \sigma_2 + \Delta\sigma_2) \tag{5}$$

where, $\Delta\theta = (\Delta\omega, \Delta\sigma_1, \Delta\sigma_2)$ denotes the modified parameter value θ . Then the modified parameter value increases the overbounding to be gradually conservative. Before estimating the overbounding module through the Louis algorithm stimulated through previous results, it is essential to validate whether there is a convergence possibility equivalent to nominal confidence. Hypothetically considering an uncertainty, the probable error sources and qualification of module error are critical. The empirical distribution functions converge to primary CDF via the overall probability of whether the sample size is appropriately huge. This is done through experimental circulation of restricted samples dissimilar to the primary distribution. The module error rises mostly due to the limited number of components. However, GMM is a real model with an enlarging component which is controlled in practical environment applications, approximately. Therefore, in (4) comparatively estimates sample data more than the accurate estimation. The selected parameter of a correct parametric is presented in Table 1. Another model violates a GMM which is known as false parametric. If a correct estimation is precise while a false module is imprecise, then an existing error is tested. The selected parameter of a false parametric is presented in Table 2. The MC simulation process is presented in Figure 3.

Table 1. The selected parameter of the correct parametric model

Parameter	ω_1	σ_1	σ_2
1	0.85	1.82	0.75
Group 2	0.95	0.97	0.11
3	0.975	1.50	0.30
4	0.50	1.50	0.50

Table 2. The selected parameter of the false parametric model

Distribution	NIG	GCET	GPO	Stable
Parameter	$\alpha = 0.65$ $\beta = 0$ $\sigma = 0.65$ $\mu = 0$	$El = 1.57$ $\sigma = 0.8$	$\sigma = 0.82$ $\gamma = 0.03$	$\alpha = 1.95$ $\beta = 0$ $\sigma = 0.9$ $\mu = 0$

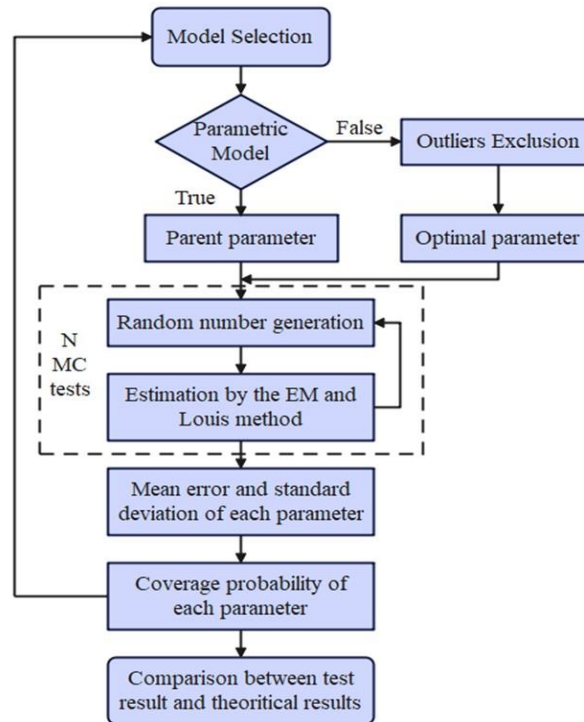


Figure 3. Flowchart of MC simulation process

Additionally, the correct estimation of Bayesian GMM is determined. For a correct parametric module, the accurate estimation is called a parent parameter which is defined as corresponding to the primary distribution directly. For a false parametric module, Bayesian GMM primary distribution is shorter. The optimum range is estimated through the decreased selected cost function for replacing the parent parameter which is represented as (6),

$$(\omega_{opt}, \sigma_{1,opt}, \sigma_{2,opt}) = \underset{\omega, \sigma_1, \sigma_2}{\operatorname{argmin}} \int_{-\infty}^{\infty} |F(Z; \omega, \sigma_1, \sigma_2) - G(Z)| dz \quad (6)$$

where, $G(Z)$ is the sample's primary distribution. $F(Z; \omega, \sigma_1, \sigma_2)$ is the CDF of Bayesian GMM. Most significantly, these parameters are inadequately decided through primary distributions. In total, thousands of Monte Carlo (MC) experimentations [27] are followed through later choosing parameters and distributions. In Figure 3, the upper loop defines the model type in which every model produces 2500 individual samples. Later, the true value probability named as coverage probability dropping in the specified assurance level is defined. Atlast, the sample type is restored and this procedure is repeated until all simulations.

3.4. Ifree-based REOM formation

The convolution is essential for attaining Ifree-based overbounding where individual-frequency overbounding unlocks the below convolution, and the output according to mathematical estimation neglects any obvious distribution. Therefore, overbounding data is unable to broadcast through restricted parameters over the signal route. The scientific characteristics of distribution overbounding are essential. The overbounding Ifree-based error and distribution model of every frequency is represented in (7),

$$p_{OB,i}(y) = \omega_{i,1}\varphi(y; 0, \sigma_{i,1}) + \omega_{i,2}\varphi(y; 0, \sigma_{i,2}) \quad (7)$$

where, $i = 1$ and 2 denote various frequencies. Considering that the Ifree measurement errors are individual, the overbounding is preserved for the later convolution procedure.

3.5. Ifree-based protection level estimation using GMM overbounds

For ensuring integrity, the GBAS protection levels are deployed in position while the error distribution feature parameters are broadcast in a range [28]. Hence, project overbounding into the protection level is crucial to verify the truthfulness. The vertical error is higher than lateral error, then vertical protection is considered as a sample. The position error E_v is linear integration error for each employed satellite which is shown in (8),

$$E_v = \sum_{k=1}^N S_{3,k} E_k \quad (8)$$

Here, $S_{3,k}$ is the k th row element's vertical-position of estimation matrix S , while N is the quantity of visual satellites. E_k is k th error equivalent satellite covering every error source range which includes noise, tropospheric and multipath errors. Subsequently, the probability density of position error is defined through GBAS range errors. The GMM calculates the accurate observations by means of the Gaussian possibility densities. Every GMM comprises of K Gaussian distributions, then every observation q have the distributions as numerically presented in (9),

$$P(q_i | \pi, \mu, \gamma) = \sum_{j=1}^K \pi_j N(q_i | \mu_j, \gamma_j^{-1}) \quad (9)$$

where, q_i is a low-dimensional data attained through an autoencoder, $\mu = \{\mu_j\}$, $\gamma = \{\gamma_j\}$ and $\pi = \{\pi_j\}$ respectively are the mean, covariance matrix and mixing coefficient. $\sum_{j=1}^K \pi_j = 1$, then the observation is attained through the (10) and (11),

$$c_i \sim \text{categorical}(\pi_1, \pi_2, \dots, \pi_k), \quad (10)$$

$$p_i | c_i \sim N(\mu_{ci}, \gamma_{ci}^{-1}), \quad (11)$$

This paper presents the GMM into a Bayesian GMM through mean, coefficient mixture and covariance matrix taken as latent variable in the prior distribution as represented numerically in (12),

$$P(\pi_1, \pi_2, \dots, \pi_K | \alpha_0) = \frac{\Gamma(K\alpha_0)}{[\Gamma(\alpha_0)]^K} \pi_1^{\alpha_0-1} \dots \pi_K^{\alpha_0-1}, \quad (12)$$

where, α_0 is a concentration parameter, the value of mixing coefficient is near to zero and $\Gamma(x)$ is a Gamma function. The mean and covariance matrix are sampled through the (13),

$$P(\mu_j | \gamma_j) = N(\mu_j | \beta_0 (\eta_0 \gamma_j)^{-1}) W(\gamma_j | v_0, \sigma_0), \quad (13)$$

Hence, the processes involved in Bayesian GMM generation for every observation are presented in (14), (15), (16) and (17),

$$\pi_1, \dots, \pi_k \sim \text{Dir}(\alpha_0), \quad (14)$$

$$c_i \sim \text{categorical}(\pi_1, \dots, \pi_k), \quad (15)$$

$$(\mu_j | \gamma_j) \sim \text{NW}(\beta_0, \eta_0, v_0, \sigma_0), \quad (16)$$

$$p_i | c_i \sim N(\mu_{c_i}, \gamma_{c_i}^{-1}), \quad (17)$$

The traditional GMM employs expectation maximization (EM) to solve the parameters iteratively, but the EM does not find the optimum global solution continuously and it specifies the number of clusters. So, the Bayesian GMM is employed to solve these issues.

4. RESULTS AND DISCUSSION

4.1. Effects of error sources

The major error sources affect the position by applying IFree-based GBAS range errors according to GMM like satellite position, velocity error, and clock drift. The user position and attitude error effects are described in the below subsections. The attained results illustrate that the user positions are susceptible to satellite positions. Likewise, the attitude error is susceptible to satellite positions and invulnerable to velocity errors and clock drift.

4.1.1. Satellite position error

The position error is included at the top of the baseline which comprises thermal noise due to which, every position consumes a fixed error on it. Tables 3 and 4 show the position error on the root mean square error (RMSE) position and the RMSE attitude. The position error increases for an intermediate of 2.5 km in position error and extends for a worst of 4.4 km. The attitude error degrades through the intermediate of 0.72° in position error based on noise. The degradation of attitude error improves to the worst case of 1.87° .

Table 3. Influence of position error on RMSE position

Satellite Axis	Satellite effects		
	Noise	Intermediate	Worst
X	100	1,300	2,400
Y	80	1,100	2,200
Z	200	1,500	2,600

Table 4. Influence of position error on RMSE attitude

Satellite Dimension	Satellite effects		
	Noise	Intermediate	Worst
roll	1.0	1.5	1.8
pitch	1.6	2.0	2.4
yaw	3.0	3.5	5.0

4.1.2. Satellite velocity error

This error alters shift prediction and the output affects navigation evaluation. The position error is included in the upper baseline which encompasses thermal noise. Because of this issue, every position consumes fixed error on it. Tables 5 and 6 illustrate the velocity error on RMSE position and attitude. The position error is degraded to an intermediate of 273 m based on noise. The degeneration achieves a worst case of 1.09 km.

Table 5. Influence of velocity error on RMSE position

Satellite Axis	Satellite effects		
	Noise	Intermediate	Worst
X	100	300	800
Y	50	180	500
Z	150	250	600

Table 6. Influence of velocity error on RMSE attitude

Satellite Dimension	Satellite effects		
	Noise	Intermediate	Worst
roll	1.2	1.2	1.4
pitch	1.5	1.5	1.8
yaw	3.5	3.5	3.8

4.1.3. Satellite clock drift

The guideline encompasses thermal noise which is attached to fixed satellite clock drift. Consider every satellite value randomly utilizing a gaussian distribution through the standard deviation for the intermediate and worst case of 1ppb and 10ppb, correspondingly. Tables 7 and 8 show the clock drift on RMSE position and RMSE attitude, respectively.

Table 7. Influence of clock drift on RMSE position

Satellite Axis	Satellite effects		
	Noise	Intermediate	Worst
X	80	150	1,000
Y	50	100	900
Z	150	180	1,100

Table 8. Influence of clock drift on RMSE attitude

Satellite Dimension	Satellite effects		
	Noise	Intermediate	Worst
roll	1.0	1.0	1.2
pitch	1.3	1.3	1.6
Yaw	3.3	3.3	3.6

4.2. Comparative analysis

This section shows the comparative analysis of the proposed overbounding process for Ifree-based GBAS range error based on GMM in terms of satellite position, velocity error and clock drift, as shown in Table 9. The satellite position, velocity error, and clock drift of the existing method [25] are assessed for estimating the ability of the suggested method. The suggested method achieves better results on all three parameters with three satellite effects like noise, intermediate and worst cases.

Table 9. Comparative analysis of the proposed method with the existing method

Effects of error sources	Author	Noise		Intermediate		Worst	
		Position error (m)	Attitude error (°)	Position error (m)	Attitude error (°)	Position error (m)	Attitude error (°)
Satellite position error	Jardak and Jault [25]	190.0	2.70	1,533	8.90	2,566	3.60
	Proposed method	126.6	1.86	1,300	2.33	2,400	3.06
Satellite velocity error	Jardak and Jault [25]	146.6	2.60	266.6	7.80	723.3	2.83
	Proposed method	100.0	2.06	243.3	2.06	633.3	4.46
Satellite clock drift	Jardak and Jault [25]	126.6	2.63	183.3	2.63	1,166	2.93
	Proposed method	93.33	1.86	143.3	1.86	1,000	2.13

5. CONCLUSION

The Ifree-based filtering technique efficiently mitigates the GBAS ionospheric anomalies as it amplifies noise and affects obtainability. To increase the availability, this paper recommends an overbounding process for Ifree-based GBAS range error according to Bayesian GMM. In order to fit heavy-tailed and single-frequency error, a dual-component Bayesian GMM model is recognized. The general ambiguity estimation method is established through the MC test. Moreover, the nonparametric technique is employed to remunerate for this erroneousness. According to the property of convolution invariance, the vertical protection level in the position field is determined without presenting difficult numerical calculations. This research study characterizes the performance of both position and attitude to the satellite position, velocity error and clock drift. This enables the understanding and evaluation of every error source's contribution to the navigation errors. Future work will be carried out to improve the augmentation process using Bayesian GMM overbounds.




REFERENCES

- [1] Z. Gao, K. Fang, Y. Zhu, Z. Wang, and K. Guo, "An ionospheric anomaly monitor based on the one class support vector algorithm for the ground-based augmentation system," *Remote Sensing*, vol. 13, no. 21, Oct. 2021, doi: 10.3390/rs13214327.
- [2] X. Li *et al.*, "Single-frequency cycle slip detection and repair based on Doppler residuals with inertial aiding for ground-based navigation systems," *GPS Solutions*, vol. 26, no. 4, Oct. 2022, doi: 10.1007/s10291-022-01297-1.
- [3] S. Sophan, L. M. M. Myint, S. Saito, and P. Supnithi, "Performance improvement of the GAGAN satellite-based augmentation system based on local ionospheric delay estimation in Thailand," *GPS Solutions*, vol. 26, no. 4, Oct. 2022, doi: 10.1007/s10291-022-01293-5.
- [4] K. Krasuski, M. Mrozik, D. Wierzbicki, J. Ćwiklak, J. Kozuba, and A. Ciecko, "Designation of the quality of EGNOS+SDCM satellite positioning in the approach to landing procedure," *Applied Sciences*, vol. 12, no. 3, Jan. 2022, doi: 10.3390/app12031335.
- [5] M. Kim and J. Kim, "SBAS-aided GPS positioning with an extended ionosphere map at the boundaries of WAAS service area," *Remote Sensing*, vol. 13, no. 1, Jan. 2021, doi: 10.3390/rs13010151.
- [6] J. Antic, O. Maliet, and S. Trilles, "SBAS protection levels with Gauss-Markov K-factors for any integrity target," *NAVIGATION: Journal of the Institute of Navigation*, vol. 70, no. 3, May 2023, doi: 10.33012/navi.594.
- [7] A. Allahviridi-Zadeh, K. Wang, and A. El-Mowafy, "POD of small LEO satellites based on precise real-time MADOCA and SBAS-aided PPP corrections," *GPS Solutions*, vol. 25, no. 2, Apr. 2021, doi: 10.1007/s10291-020-01078-8.
- [8] T. Suzuki and Y. Amano, "NLOS multipath classification of GNSS signal correlation output using machine learning," *Sensors*, vol. 21, no. 7, Apr. 2021, doi: 10.3390/s21072503.
- [9] Z. Guo *et al.*, "The extraction and characterization of pseudorange multipath based on BDS-3 multi-frequency observations," *Sensors*, vol. 23, no. 13, Jul. 2023, doi: 10.3390/s23136151.
- [10] X. Dai, C. Ke, Q. Quan, and K.-Y. Cai, "RFlySim: automatic test platform for UAV autopilot systems with FPGA-based hardware-in-the-loop simulations," *Aerospace Science and Technology*, vol. 114, Jul. 2021, doi: 10.1016/j.ast.2021.106727.
- [11] X. Zou *et al.*, "Multipath error fusion modeling methods for multi-GNSS," *Remote Sensing*, vol. 13, no. 15, Jul. 2021, doi: 10.3390/rs13152925.




- [12] Q. Liu *et al.*, “Retrieval of soil moisture content based on multisatellite dual-frequency combination multipath errors,” *Sensors*, vol. 22, no. 4, Feb. 2022, doi: 10.3390/s22041611.
- [13] L.-C. Tsai *et al.*, “Ocean-surface wave measurements using scintillation theories on seaborne software-defined GPS and SBAS reflectometry observations,” *Sensors*, vol. 23, no. 13, Jul. 2023, doi: 10.3390/s23136185.
- [14] W. Li *et al.*, “A satellite-based method for modeling ionospheric slant TEC from GNSS observations: algorithm and validation,” *GPS Solutions*, vol. 26, no. 1, Jan. 2022, doi: 10.1007/s10291-021-01191-2.
- [15] F. Paredes-Trejo *et al.*, “Drought assessment in the São Francisco river basin using satellite-based and ground-based indices,” *Remote Sensing*, vol. 13, no. 19, Sep. 2021, doi: 10.3390/rs13193921.
- [16] A. Hussain, H. Magsi, A. Ahmed, H. Hussain, Z. H. Khand, and F. Akhtar, “The effects of using variable lengths for degraded signal acquisition in GPS receivers,” *International Journal of Electrical and Computer Engineering (IJECE)*, vol. 11, no. 4, Aug. 2021, doi: 10.11591/ijece.v11i4.pp3201-3211.
- [17] K. M. Ng, R. S. Nahar, and M. IbneReaz, “Linear regression models with autoregressive integrated moving average errors for measurements from real time kinematics-global navigation satellite system during dynamic test,” *International Journal of Electrical and Computer Engineering (IJECE)*, vol. 13, no. 1, Feb. 2023, doi: 10.11591/ijece.v13i1.pp770-780.
- [18] Z. Abidin, N. Aryawiratama, A. Muttaqin, and R. Miyauchi, “Design of field programmable gate array-based data processing system for multi global positioning system receiver,” *International Journal of Electrical and Computer Engineering (IJECE)*, vol. 12, no. 4, pp. 3466–3476, Aug. 2022, doi: 10.11591/ijece.v12i4.pp3466-3476.
- [19] Z. Gao, K. Fang, Z. Wang, K. Guo, and Y. Liu, “An error overbounding method based on a Gaussian mixture model with uncertainty estimation for a dual-frequency ground-based augmentation system,” *Remote Sensing*, vol. 14, no. 5, Feb. 2022, doi: 10.3390/rs14051111.
- [20] H. Lee, S. Pullen, J. Lee, B. Park, M. Yoon, and J. Seo, “Optimal parameter inflation to enhance the availability of single-frequency GBAS for intelligent air transportation,” *IEEE Transactions on Intelligent Transportation Systems*, vol. 23, no. 10, pp. 17801–17808, Oct. 2022, doi: 10.1109/TITS.2022.3157138.
- [21] N. Maurer *et al.*, “Flight trial demonstration of secure GBAS via the I-band digital aeronautical communications system (LDACS),” *IEEE Aerospace and Electronic Systems Magazine*, vol. 36, no. 4, pp. 8–17, Apr. 2021, doi: 10.1109/MAES.2021.3052318.
- [22] H.-B. Lee, K.-H. Kwon, and J.-H. Won, “Feasibility analysis of GPS L2C signals for SSV receivers on SBAS GEO satellites,” *Remote Sensing*, vol. 14, no. 21, Oct. 2022, doi: 10.3390/rs14215329.
- [23] E. Bang and J. Lee, “Undersampled ionospheric irregularity threat parameterization using a three-dimensional model for satellite-based augmentation systems,” *IEEE Transactions on Aerospace and Electronic Systems*, pp. 1–24, 2022, doi: 10.1109/TAES.2022.3199192.
- [24] X. Wang, X. Cui, G. Liu, and M. Lu, “Designing the signal quality monitoring algorithm based on chip domain observables for BDS B1C/B2a signals under the requirements of DFMC SBAS,” *Remote Sensing*, vol. 15, no. 4, Feb. 2023, doi: 10.3390/rs15041008.
- [25] N. Jardak and Q. Jault, “The potential of LEO satellite-based opportunistic navigation for high dynamic applications,” *Sensors*, vol. 22, no. 7, Mar. 2022, doi: 10.3390/s22072541.
- [26] G. Alomani and M. Kayid, “Stochastic properties of fractional generalized cumulative residual entropy and its extensions,” *Entropy*, vol. 24, no. 8, Jul. 2022, doi: 10.3390/e24081041.
- [27] J. Sobieraj and D. Metelski, “Project risk in the context of construction schedules-combined Monte Carlo simulation and time at risk (TaR) approach: insights from the fort bema housing estate complex,” *Applied Sciences*, vol. 12, no. 3, Jan. 2022, doi: 10.3390/app12031044.
- [28] Y. Wang, J. Zhao, S. Hao, S. Hui, and B. Yu, “Optimization of protection level of GBAS with Gaussian mixture model,” *Electronics*, vol. 12, no. 15, Jul. 2023, doi: 10.3390/electronics12153290.

BIOGRAPHIES OF AUTHORS



Sheher Banu    joined MVJ College of Engineering, Department of Electronics and Communication Engineering as an assistant professor in 2016. Pursuing Ph.D. from Visvesvaraya Technological University, India since 2018. I have 10+ years of work experience, completed M.Tech in digital communication and networking and B.E in instrumentation technology. My areas of interest are signal processing, sensor technology, instrumentation, global positioning systems, and navigation. She can be contacted at email: sheherbanu@mvjce.edu.in.



Hameem Shanavas    is professor, and currently the Dean in MVJCE, Bangalore. He completed his bachelor’s degree in electronics and communication (2006), Masters in VLSI design (2008), Masters in business administration (2009) and PhD (2015) from Anna University, Chennai. He has published in 40 journals and attended 30 National and International Conferences. He can be contacted at email: hameemshan@gmail.com.